33rd Annual International Conference of the IEEE EMBS
Boston, Massachusetts USA, August 30 - September 3, 2011

Dual Inductive Link Coil Design for a Neural Recording System

Alexander Rush, Student *Member, IEEE, EMBS*, Philip R. Troyk, *Senior Member, IEEE*

***Abstract*—This paper reports an approach to the physical design of the coils used in a dual inductive link to provide two-way wireless communication and power for a neural recording system. The design approach makes use of an analytic model of the link performance in terms of the physical parameters of the link, which allows physical parameters to be iterated on a computer rather than on the bench to find the optimal design within the physical restrictions imposed. In particular, this approach was used to choose the optimal implant data coil sizing to maximize the difference between the contributions of the constructive and destructive paths of the reverse telemetry signal.**

I. Introduction

A wireless neural recording system requires power and forward data to be transferred to the implant. Both power and forward data can be implemented on a single inductive link, with forward data encoded as modulation of the power carrier. Reverse telemetry can be achieved on the same link by a method called load shift keying (LSK), but the data rate is generally limited to a fraction of the power carrier frequency, which is typically in the low MHz range. Furthermore, if multiple implants are powered by the external power coil, an external controller must time-division multiplex (TDM) the reverse telemetry from the implants. To send raw neural data from 16 channels, which is our initial goal, assuming an ADC resolution of 10bits/sample and a sampling rate of 20kSamples/s, a reverse telemetry data rate of at least 3.2Mbps would be required.

Therefore, it is desirable to have another inductive link for reverse telemetry. For compactness these inductive links should operate in the same space, but to do so one must consider interactions between the power and data coils, because destructive paths of the reverse telemetry signal (out of phase with the constructive paths) can greatly reduce the amplitude of the signal received by the external data coil. Such an approach was taken by [1] for the design of a dual inductive link for power and forward data transmission for a retinal prosthesis.

Manuscript received April 15, 2011.

A. Rush is with the Illinois Institute of Technology, Chicago, IL 60616 USA (e-mail: rushale@iit.edu).

P. R. Troyk, is with Illinois Institute of Technology, Chicago, IL 60616 USA (e-mail: troyk@iit.edu).

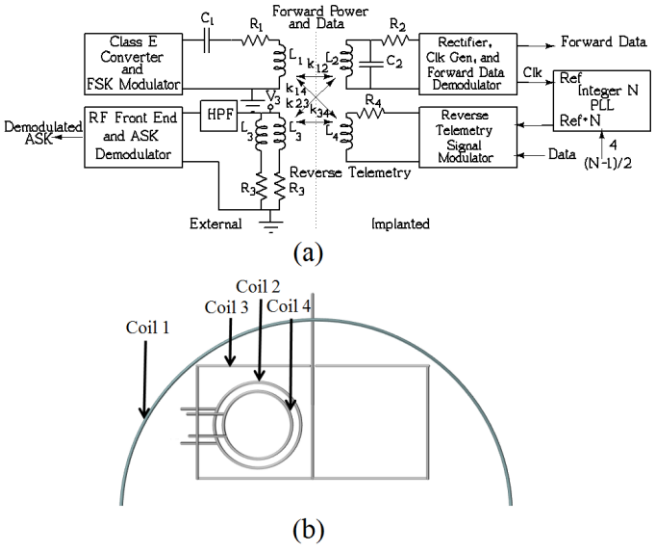

Figure 1. (a) Schematic of bidirectional data transfer system (b) Physical diagram of dual inductive link coils

Design of both the power and data inductive links can be facilitated with the help of an analytic model of the inductive link electrical and performance parameters in terms of the link physical parameters [2-4]. This allows the physical parameters to be iterated on a computer rather than on the bench to find the optimal design within the physical restriction imposed. An analytic model of the link was used here to find the data coil radius which maximizes the difference between the contributions of the constructive and destructive reverse telemetry signal paths in order to maximize the amplitude of the data signal received on the external data coil. Other challenges associated with a dual inductive link, including interference from the power carrier harmonics upon the data link as well as ways to reduce and mitigate this interference are discussed in a companion paper [5].

II. Coil Arrangement

Here we report a dual inductive link for wireless power and bidirectional data transfer system illustrated in Fig. 1a. The physical arrangement of the coils is illustrated in Fig. 1b.

Power transfer to the implant is achieved by generating a large AC current in the external power coil, referred to here as coil 1, using a class E converter. AC voltage is induced in the implanted power coil, referred to here as coil 2, proportional to the coupling coefficient between the external and implanted power coils, k_{12}. This AC voltage is rectified to supply the chip with power and is used to generate a reference clock for the implant. Forward data transfer is achieved by modulation of the 5MHz power carrier at a data rate of 1.25Mbps to send control data to the implant.

In the implant circuitry, the reference clock, derived from the 5MHz power carrier, is spun up by an integer-N PLL to generate a reverse telemetry carrier between 50MHz and 100MHz. The reverse telemetry is either ASK or BPSK modulated. Driver circuitry induces current in implanted data coil, which is concentric to the implanted power coil, to generate the reverse telemetry signal. According to simulation, with a power supply of 3V, the driver circuitry can drive 2mA peak current in the implant data coil, referred to here as coil 4.

Data is received by one of the external differential data coils, referred to here as coil 3, with inductance L_3 and effective series resistance R_3. A differential coil configuration is used to cancel the large power signal at its fundamental frequency as well as harmonics generated by the class E converter and falling within the frequency range of the reverse telemetry.

III. Analytic Model

A dual coil link for power and reverse telemetry, illustrated in Fig. 1, can be optimized with an algorithm which iterates the modifiable link parameters and chooses the combination of physical parameters which is associated with the best performance as predicted by an analytic model of the link.

This algorithm uses an expression similar to that presented in [1] for a dual coil system to provide power and forward telemetry to a retinal prosthesis. The expression was adapted for a dual coil system to provide power and reverse telemetry. The variables used for the electrical parameters of the link are the same as illustrated in Fig. 1.

The derivation is similar to [1], and space does not allow it to be included here. The assumptions critical to the derivation of the simplified equation for data magnitude, (1), are high quality factor coils and that the power coils see a short circuit at the data carrier frequency. This expression for the magnitude of the reverse telemetry signal received by the external data coil, V_3, shown in Fig. 1a is

$$V_3 = -I_4 j\omega_{data} k_{eff} \sqrt{L_3 L_4} \quad (1)$$

$$k_{eff} = k_{34} - k_{24}k_{23} - k_{14}k_{13} + k_{14}k_{12}k_{23} + k_{24}k_{12}k_{13}$$

where I_4 is the current induced in the implant data coil by the coil driver circuitry, ω_{data} is the angular frequency of the reverse telemetry carrier, and L_3, L_4, k_{12}, k_{13}, etc. are as indicated in Fig. 1. According to this result, the data link can be optimized by maximizing the effective coupling coefficient, k_{eff}. By analyzing the dual coil link with this equation for k_{eff}, we found that the optimal ratio of implanted power and data coil radii for our design was close to 0.8.

To raise confidence in k_{eff} as a performance metric, we compared values of V_3 simulated in Orcad to values of V_3 calculated using this equation for ten values of implanted data coil radius, fixing all other physical parameters. A realistic power link and external data coil were assumed for simulation, including values calculated for coil effective series resistance, inductance, and self-capacitance. The physical parameters which were assumed for this plot, while the radius of the implanted data coil was varied, are summarized in Table I. The current in the data coil was modeled as sinusoidal with a peak amplitude of 1mA.

One can see from Fig. 2 that the simulated values for V_3 using realistic coil parameters (inductance, effective series resistance, etc.) closely match the calculated values for V_3. Based on this data, we chose 8mm as the optimal diameter for an implanted data coil for the 10mm power coil assumed.

A. Self-Capacitance

Self-capacitance is often a limiting factor in the design of high quality factor coils. In general, the quality factor increases with turns, but, at some point, the self-capacitance becomes too large for the coil to operate in the desired range. A large self-capacitance means a low self-resonant frequency, above which the coil behaves like a capacitor.

Expressions for exact self-capacitance calculation have eluded researchers leading some to resort to finite-element modeling, which though much slower provides better estimates of the first self-resonant frequency and can take into account effects that expressions for self-capacitance do not.

One old analysis by [6] calculates self-capacitance of single- and multi-layer coils using the principal:

$$C_e = C\left(\frac{E_1^2}{E_2^2}\right) \quad (2)$$

where E_1 is the volts across some capacitance C, and E_2 is the reference voltage at which C has the effective value of Ce. This approach is supported by a separate derivation by [4] which arrives at this result by making the same simplifying assumption as [6], i.e. that the flux through each turn in the coil is the same. [4] gives the following expression for self-capacitance:

$$C_{self} = \sum_{p<k} \left(\frac{k-p}{N_t}\right)^2 C_{p,k} \quad (3)$$

where N_t is the total number of turns in the coil and $C_{p,k}$ is the parasitic capacitance between nodes p and k.

For computing turn-to-turn capacitance, [4] used expressions derived by [7]. These expressions were slightly modified by [7] to allow for turn-to-turn and layer-to-layer spacing. The approximate expression for turn-to-turn capacitance derived by [6] is

$$C_{tt} = \varepsilon_0 l_t \int_0^{\theta_{max}/2} \frac{1}{1+\frac{1}{\varepsilon_r} ln\frac{D_0}{D_c} - cos\theta} d\theta \quad (4)$$

where Dc is the diameter of the conductor without coating, Do is the diameter of the conductor with coating, and l_t is the turn length, and Θ_{max} is the angle between adjacent conductors which contributes to the turn-to-turn capacitance. We and [4] used $\pi/2$, whereas [7] used $\pi/3$. However, [7] showed that the capacitance/radian becomes quite small for moderately large angles, so the resulting difference in computed values of self-capacitance is small.

Using this method the implant power coil, coil 2, was computed to have a self-capacitance of 4.90pF, while the measured value of self-capacitance was 5.21pF (6% error). The measured value of self-capacitance was determined by measuring the first self-resonant frequency (SRF) of the coil, measuring the self-inductance of the coil, computing the effective parallel capacitance, and subtracting the measured parasitic capacitance on the test-board. Because the implant data coil, coil 4, is a single-layer coil with several turns, its self-capacitance is dwarfed by parasitic capacitance in the test-setup and the coupled self-capacitance of L_4. The calculated value of the self-capacitance of L_4 is 50.8fF.

B. Self and Mutual Inductance

The inductance calculations were made by summing the self-inductance of each turn in a coil and its mutual inductance to every other turn in the coil. The computation time was reduced greatly by not re-computing the mutual and self-inductances which are the same but instead using the appropriate integer factor to represent the multiplicity. A simple expression for self-inductance, L_a, which gives the same result as the algorithm we implemented to compute inductance is

$$L_a = \sum_{i=1}^{N_a} L(a_i, R, d_{i,j,k,l}) + \sum_{i=1}^{nl_a} \sum_{j=1}^{N_a/nl_a} \sum_{k=1}^{nl_a} \sum_{l=1}^{N_a/nl_a} M(a_i, a_k) * (1 - \delta_{i,j,k,l}) \quad (5)$$

where L is the inductance of a single turn, nl is the number of layers in coil a, N_a is the number of turns in coil a, a_i is the radius corresponding to row i, a_k is the radius corresponding to row k, and R is the radius of the conducting part of the wire, M is the mutual inductance between two turns, $d_{i,j,k,l}$ is the axial distance between turn i,j and turn k,l. $\delta_{i,j,k,l} = 1$ for i,j=k,l, and $\delta_{i,j,k,l} = 0$ otherwise.

For computing inductance and coupling coefficient, Maxwell's original equation for the mutual inductance between circles was used [8,9]. In the case of axial misalignment between coils, an expression given in [9] can be used. To compute the self-inductance of a single circular turn of wire, Kirchoff's formula provided in [8] was used. To compute the self-inductance of the single-turn external data coil, an equation for the self-inductance of a rectangle with a rectangular cross-section was used, which was provided in [8]. Space does not allow the four equations mentioned in this paragraph to be included here.

The inductance of the external power coil listed in Table I was measured from an existing class E inductor in use. To greatly simplify the equations used to compute coupling, the bucking coils, which are two square inductors side-by-side, are modeled as a single circular inductor with the same area as one of the two square inductors. We considered modeling the bucking coil as a single coil a reasonable approximation because if the implanted data coil is coaxial with one of the two bucking coils, then the coupling to the non-coaxial bucking coils is much less than to the coaxial bucking coil.

When computing the coupling coefficient between the implanted coils, k_{24}, for nearly equal radii, the winding depth and traverse length have a significant effect on the coupling coefficient, and the wires in one coil cannot be approximated as all having the same distance to the wires in the other coil. Therefore, for improved accuracy, and because the computation time was not prohibitively large, the mutual inductance was computed by taking the sum of the mutual inductance between each wire in one coil and all others in the other coil. The mutual inductance between each pair of circles was computed using Maxwell's original equation for the mutual inductance between two circles. The computed value of k_{24} using this approach was 0.41, and the measured value was 0.38.

A simple expression for mutual-inductance, L_a, which gives the same result as the algorithm we implemented to compute mutual-inductance is

$$M_{a,b} = \sum_{i=1}^{nl_a} \sum_{j=1}^{N_a/nl_a} \sum_{k=1}^{nl_b} \sum_{l=1}^{N_b/nl_b} M(a_i, a_k, d_{i,j,k,l}) \quad (6)$$

The coupling coefficient between coils a and b is related to the mutual inductance, $M_{a,b}$, by the expression

$$k_{a,b} = \frac{M_{a,b}}{\sqrt{L_a L_b}} \quad (7)$$

C. Effective Series Resistance

The effective series resistance (ESR) is an important value because it helps to determine the maximum power transmission distance as well as a portion of the power dissipated within the biological environment. However, we have found that it is very difficult to accurately predict.

The ESR is affected by both skin effect, the tendency of current to flow at the surface of a conductor at high frequencies, and proximity effect, current crowding in a conductor due to nearby current-carrying conductors. For multilayer coils with a wire diameter smaller than the skin depth, the latter phenomenon has a greater effect upon the ESR. We first tried to predict the ESR using approximate analytic expressions from [10] but abandoned this method in favor of the well known Dowell Method [11], characterized by its low computational intensity. According to [10], the traditional Dowell Method should be sufficiently accurate

for our application, based on the ratio of the wire size to the skin depth of the current flowing in the wire.

TABLE I. PHYSICAL PARAMETERS ASSUMED FOR DESIGN

Coil 1		**Coil 2**		**Coil 3**	
Length	9 mm	Wire Diameter	25 µm	Turns	1
Turns	7	Insulation Thickness	5 µm	Number of Layers	1
Inductance	4.62 µH	Turns Per Layer	12	Length	15 mm
Radius	3 cm	Number of Layers	3	Width	19 mm
		Radius	5 mm	Trace Width	0.51 mm

IV. COIL FABRICATION AND MEASUREMENT

In order to facilitate measurement of the dual coil link electrical parameters as well as to facilitate testing of the dual coil link performance we fabricated a coil form for winding the prototype concentric coplanar implanted data coils.

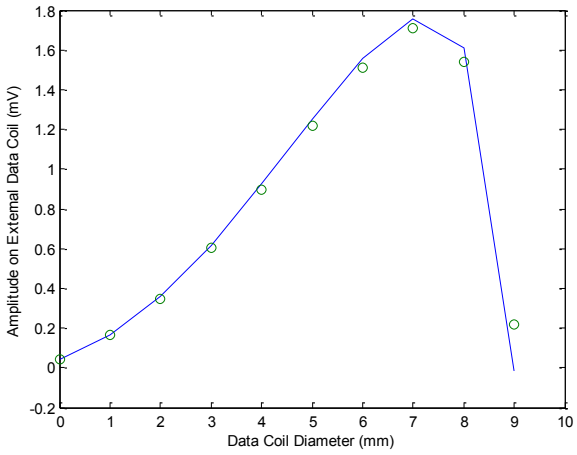

Figure 2. Comparison of simulated values for reverse telemetry data signal amplitude using realistic coil parameters (inductance, effective series resistance, etc.) and the values calculated using (1), which was derived with simplifying assumptions.

The data coil and power coil were wound with 50AWG gold wire and wire bonded to a PCB for testing of electrical parameters and interfacing with the implant circuitry. Because inductance and coupling coefficient are determined by coil geometry, these parameters were measured at low frequency with a Solartron HP 1260 Impedance/Gain-Phase Analyzer. The measured and theoretical values of the coil inductance are given Table. 2.

Many link electrical parameter measurements have not yet been made including, k_{12}, k_{34} as a function of distance, and coil effective series resistance as a function of frequency. These measurements will be made with an Agilent 8753C Vector Network Analyzer and test boards designed to minimize parasitics, as well as a custom XYZ positioning system, which has been fabricated for testing the dual inductive link system.

TABLE II. INDUCTANCE VALUES

Electrical Parameter	**Theoretical**	**Measured**
L_1	—	4.62µH
L_2	31.7 µH	32.4µH
L_3	57.3nH	55nH
L_4	2.76uH	2.98uH

V. CONCLUSION

This paper presents a method for optimizing implant coil sizing when a coaxial coil arrangement is used. This method makes use of an analytic description of the link performance, here the amplitude of reverse telemetry received by the external data coil, in terms of the physical parameters of the link. This analytic model allows iteration of link physical parameters on a computer rather than on the bench to find an optimal link design within the physical restrictions imposed.

REFERENCES

[1] G.Wang, W. Liu, M. Sivaprakasam, M. Zhou, J. Weiland, M. Humayun, "A Dual Band Wireless Power and Data Telemetry for Retinal Prosthesis," *Proceedings of the28th IEEE EMBS Annual International Conference* , pp. 4392-4395, Aug. 2006.

[2] U.M. Jow, M. Ghovanloo, "Modeling and Optimization of Printed Spiral Coils in Air, Saline, and Muscle Tissue Environments," *Proceedings of the31st IEEE EMBS Annual International Conference*, pp. 6387-6390, Sep. 2009.

[3] P.R. Troyk, A. Rush,. "Inductive Link Design for Miniature Implants," *Proceedings of the 31st Annual International Conference of the IEEE EMBS*, pp. 204-209, Sep. 2009.

[4] Z. Yang, W. Liu, E. Basham, "Inductor Modeling in Wireless Links for Implantable Electronics," IEEE Transactions on Magnetics, vol. 43, no. 10, pp. 3851-3860, Oct. 2007.

[5] P.R. Troyk, A. Rush,. "Electronic Performance of a Dual Inductive Link for a Wireless Neural Recording Implant," *Proceedings of the 33rd Annual International Conference of the IEEE EMBS*, Sep. 2011.

[6] L. Reuben, *Electronic Transformers and Circuit.* Wiley, 1947.

[7] A. Massrini, M. Kazimierczuk, "Self-Capacitance of Inductors," IEEE Transactions on Power Electronics, vol. 12, no. 4, pp. 671-676, Jul. 1997.

[8] E.B. Rosa, "No 169 – Formulas and Tables for the Calculation of Mutual and Self Inductance," Scientific Papers of the Bureau of Standards, 1911.

[9] Zierhofer, Clemens M. "High-Efficiency Coupling-Insensitive Transcutaneous Power and Data Transmission Via an Inductive Link." IEEE Transactions on Biomedical Engineering 37 (1990): 716-721.

[10] X. Nan and C.R. Sullivan, "An improved calculation of proximity effect loss in high frequency windings of round conductors," in Proceedings of the IEEE Power Electronics Specialists Conference, 2003, vol. 2, pp. 853–860, 2003.

[11] P.L. Dowell, "Effects of eddy currents in transformer windings," Proceedings of the IEE, vol. 113, no. 8, pp. 1387–1394, Aug. 1966.